

---

# Variational Recursive Dual Filtering

---

Yuan Zhao<sup>1</sup> Il Memming Park<sup>1 2 3</sup>

## Abstract

State space models provide an interpretable framework for complex time series by combining an intuitive dynamical system model with a probabilistic observation model. We developed a flexible online learning framework for latent nonlinear state dynamics and filtered latent states. Our method utilizes the stochastic gradient variational Bayes method to jointly optimize the parameters of the nonlinear dynamics, observation model, and the black-box recognition model. Unlike previous approaches, our framework can incorporate non-trivial observation noise models and infer in real-time. We test our method on point process observations driven by continuous attractor dynamics, demonstrating its ability to recover the phase portrait, filtered trajectory, and produce long-term predictions for real-time machine learning.

## 1. Introduction

Finding interpretable structure in real-time from a streaming high-dimensional time series has many applications in science and engineering. State space models have been successful in providing a succinct description, explaining observed time series as trajectories in a low-dimensional state space. Taking a step further, state space models equipped with nonlinear dynamics provide an opportunity to describe the latent laws of the system that is generating the complex time series (Haykin & Principe, 1998; Ko & Fox, 2009; Mattos et al., 2016). Specifically, we would like to identify a continuous nonlinear process in the state space  $\mathbf{x}_t$  that captures the spatiotemporal structure of a noisy observation  $\mathbf{y}_t$ :

$$\mathbf{y}_t \sim P(\mathbf{y} | F(\mathbf{x}_t, \mathbf{u}_t)) \quad (\text{observation model}) \quad (1a)$$

$$\dot{\mathbf{x}} = G(\mathbf{x}_t, \mathbf{u}_t) \quad (\text{state dynamics}) \quad (1b)$$

---

<sup>1</sup>Department of Neurobiology and Behavior, Stony Brook University, Stony Brook, New York, USA <sup>2</sup>Department of Applied Mathematics and Statistics, Stony Brook University, Stony Brook, New York, USA <sup>3</sup>Institute for Advanced Computational Science, Stony Brook University, Stony Brook, New York, USA. Correspondence to: Il Memming Park <memming.park@stonybrook.edu>.

where  $F$  and  $G$  are continuous functions, and  $P$  denotes a probability distribution. In practice, the continuous-time state dynamics is more conveniently formulated in discrete-time as,

$$\mathbf{x}_{t+1} = \mathbf{x}_t + g(\mathbf{x}_t, \mathbf{u}_t) + \epsilon_t \quad (\text{state dynamics}) \quad (2)$$

where  $\epsilon_t$  is intended to capture unobserved perturbations of the state  $\mathbf{x}_t$ . Such continuous state space model is natural in many applications where the changes are slow and the underlying system follows physical laws and constraints (e.g., object tracking), or where learning the laws are of great interest, which is the case in neural data analysis (Roweis & Ghahramani, 2001; Mante et al., 2013; Sussillo & Barak, 2012; Frigola et al., 2014).

If the nonlinear state space model is fully specified, Bayesian inferences can estimate the latent states (either the filtering distribution  $p(\mathbf{x}_t | \mathbf{y}_{1:t})$  or the smoothing distribution  $p(\mathbf{x}_{1:t} | \mathbf{y}_{1:t})$ ), predict future states  $p(\mathbf{x}_{t:t+s} | \mathbf{y}_{1:t})$ , and predict observations  $p(\mathbf{y}_{t+1:t+s} | \mathbf{y}_{1:t})$  for  $s > 0$  (Ho & Lee, 1964; Särkkä, 2013). However, in many applications, the challenge is in learning the parameters of the state space model (a.k.a. the system identification problem). Learning both the latent state trajectory and the latent (nonlinear) state space model is known as the *dual estimation problem* (Haykin, 2001). Expectation maximization (EM) based methods have been widely used in practice (Ghahramani & Roweis, 1999; Valpola & Karhunen, 2002; Golub et al., 2013), and more recently variational autoencoder methods (Archer et al., 2015; Krishnan et al., 2015; 2017; Johnson et al., 2016; Karl et al., 2017; Watter et al., 2015) have been proposed, all of which are designed for offline analysis, and not appropriate for real-time applications. Recursive stochastic variational inference has been successful in streaming data assuming independent samples (Broderick et al., 2013), however, in the presence of temporal dependence, proposed variational algorithms (e.g., Frigola et al. (2014)) remain theoretical and untested.

In this paper, we are interested in real-time signal processing and state-space control setting (Golub et al., 2013) where we need online algorithms that can recursively solve the dual estimation problem on streaming observations. A popular solution to this problem exploits the fact that online state estimators for nonlinear state space models such as extended Kalman filter (EKF) or unscented Kalman filter (UKF) can

be used for nonlinear regression formulated as a state space model:

$$\theta_{t+1} = \theta_t + \eta_t \quad (\text{parameter}) \quad (3a)$$

$$\mathbf{z}_t = H(\mathbf{x}_t, \theta_t) + \epsilon_t \quad (\text{regression}) \quad (3b)$$

where  $H$  is a function approximator parameterized by  $\theta_t$  that maps  $\mathbf{x}$  to  $\mathbf{z}$ . Therefore, by augmenting the state space with the parameters, one can build an online dual estimator using nonlinear Kalman filtering (Wan & Van Der Merwe, 2000; Wan & Nelson, 2001). However, they involve coarse approximation of Bayesian filtering, involve many hyperparameters, do not take advantage of modern stochastic gradient optimizers, and are not easily applicable to arbitrary observation likelihoods. There are also closely related online version of EM-type algorithms (Roweis & Ghahramani, 2001) that share similar concerns. In this paper, we derive an *online* black-box variational inference framework applicable to a wide range of nonlinear state space models and observation models, that is, the computational demand of the algorithm is constant per time step.

## 2. Variational Principle for Online Dual Estimation

The crux of recursive Bayesian filtering is updating the posterior over the latent state one time step at a time.

$$p(\mathbf{x}_t | \mathbf{y}_{1:t}) = \underbrace{p(\mathbf{y}_t | \mathbf{x}_t)}_{\text{likelihood}} \underbrace{p(\mathbf{x}_t | \mathbf{y}_{1:t-1})}_{\text{prior at time } t} / \underbrace{p(\mathbf{y}_t | \mathbf{y}_{1:t-1})}_{\text{marginal likelihood}} \quad (4a)$$

$$p(\mathbf{x}_t | \mathbf{y}_{1:t-1}) = \int \underbrace{p(\mathbf{x}_t | \mathbf{x}_{t-1})}_{\text{state dynamics}} \underbrace{p(\mathbf{x}_{t-1} | \mathbf{y}_{1:t-1})}_{\text{previous posterior}} d\mathbf{x}_{t-1} \quad (4b)$$

where the input  $\mathbf{u}_t$  and parameters  $\theta$  are omitted for brevity. Unfortunately, the exact calculations of (4) are not tractable in general, especially for nonlinear dynamics models and/or non-conjugate likelihoods. We derive a recursive variational Bayesian filter by deriving an objective evidence lower bound for the marginal likelihood which is in general faster than particle filtering (Frigola et al., 2014). Let  $q(\mathbf{x}_t)$  denote an arbitrary probability measure which will eventually approximate the filtering density  $p(\mathbf{x}_t | \mathbf{y}_{1:t})$ . From (4a),

$$\begin{aligned} & \log p(\mathbf{y}_t | \mathbf{y}_{1:t-1}) \\ &= \mathbb{E}_{q(\mathbf{x}_t)} \left[ \log \frac{p(\mathbf{y}_t | \mathbf{x}_t) p(\mathbf{x}_t | \mathbf{y}_{1:t-1}) q(\mathbf{x}_t)}{p(\mathbf{x}_t | \mathbf{y}_{1:t}) q(\mathbf{x}_t)} \right] \\ &= \underbrace{\mathbb{E}_{q(\mathbf{x}_t)} [\log p(\mathbf{y}_t | \mathbf{x}_t)]}_{\text{reconstruction log-likelihood}} - \mathbb{D}_{\text{KL}}(q(\mathbf{x}_t) \| p(\mathbf{x}_t | \mathbf{y}_{1:t-1})) \\ & \quad + \underbrace{\mathbb{D}_{\text{KL}}(q(\mathbf{x}_t) \| p(\mathbf{x}_t | \mathbf{y}_{1:t}))}_{\text{variational gap \#1}} \end{aligned}$$

$$\begin{aligned} & \geq \mathbb{E}_{q(\mathbf{x}_t)} [\log p(\mathbf{y}_t | \mathbf{x}_t)] + \underbrace{H(q(\mathbf{x}_t))}_{\text{entropy}} \\ & \quad + \mathbb{E}_{q(\mathbf{x}_t)} [\log p(\mathbf{x}_t | \mathbf{y}_{1:t-1})] \\ &= \mathbb{E}_{q(\mathbf{x}_t)} [\log p(\mathbf{y}_t | \mathbf{x}_t)] + H(q(\mathbf{x}_t)) \\ & \quad + \mathbb{E}_{q(\mathbf{x}_t)} [\log \mathbb{E}_{p(\mathbf{x}_{t-1} | \mathbf{y}_{1:t-1})} [p(\mathbf{x}_t | \mathbf{x}_{t-1})]] \\ &= \mathbb{E}_{q(\mathbf{x}_t)} [\log p(\mathbf{y}_t | \mathbf{x}_t)] + H(q(\mathbf{x}_t)) \\ & \quad + \mathbb{E}_{q(\mathbf{x}_t)} [\mathbb{E}_{p(\mathbf{x}_{t-1} | \mathbf{y}_{1:t-1})} [\log p(\mathbf{x}_t | \mathbf{x}_{t-1})]] \\ & \quad + \underbrace{\mathbb{E}_{q(\mathbf{x}_t)} [\mathbb{D}_{\text{KL}}(p(\mathbf{x}_{t-1} | \mathbf{y}_{1:t-1}) \| p(\mathbf{x}_{t-1} | \mathbf{x}_t, \mathbf{y}_{1:t-1}))]}_{\text{variational gap \#2}} \\ & \geq \mathbb{E}_{q(\mathbf{x}_t)} [\log p(\mathbf{y}_t | \mathbf{x}_t)] + H(q(\mathbf{x}_t)) \\ & \quad + \mathbb{E}_{q(\mathbf{x}_t)} \mathbb{E}_{p(\mathbf{x}_{t-1} | \mathbf{y}_{1:t-1})} [\log p(\mathbf{x}_t | \mathbf{x}_{t-1})] \end{aligned}$$

where  $\mathbb{D}_{\text{KL}}$  denotes the Kullback-Leibler divergence. Maximizing for this lower bound would result in a variational posterior  $q(\mathbf{x}_t) \approx p(\mathbf{x}_t | \mathbf{y}_{1:t})$ . Therefore, we recursively plug in the previous step's solution to the next time step, obtaining a loss function suitable for recursive estimation:

$$\begin{aligned} \mathcal{L} := & \mathbb{E}_{q(\mathbf{x}_t)} [\log p(\mathbf{y}_t | \mathbf{x}_t)] + H(q(\mathbf{x}_t)) \\ & + \underbrace{\mathbb{E}_{q(\mathbf{x}_t)} \mathbb{E}_{q(\mathbf{x}_{t-1})} [\log p(\mathbf{x}_t | \mathbf{x}_{t-1})]}_{\text{dynamics log-likelihood}} \quad (5) \end{aligned}$$

Online variational inference is achieved by maximizing this approximate lower bound objective  $\mathcal{L}$  for the parameters of the generative model ( $p(\mathbf{y}_t | \mathbf{x}_t)$  and  $p(\mathbf{x}_t | \mathbf{x}_{t-1})$ ) and the variational posterior distribution  $q(\mathbf{x}_t)$  provided that  $q(\mathbf{x}_{t-1})$  is estimated from the previous time step. Maximizing  $\mathcal{L}$  is equivalent to minimizing the two variational gaps: (1) the variational filtering posterior has to be close to the true filtering posterior, and (2) the filtering posterior from the previous step needs to be close to  $p(\mathbf{x}_{t-1} | \mathbf{x}_t, \mathbf{y}_{1:t-1})$ . Note that this second gap is invariant to  $q(\mathbf{x}_t)$  if  $p(\mathbf{x}_{t-1} | \mathbf{x}_t, \mathbf{y}_{1:t-1}) = p(\mathbf{x}_{t-1} | \mathbf{y}_{1:t-1})$ , that is, the one-step backward smoothing distribution is identical to the filtering distribution.

On the flip side, intuitively, there are three components in  $\mathcal{L}$  that are jointly maximized: (1) **reconstruction log-likelihood** which is maximized if  $q(\mathbf{x}_t)$  concentrates around the maximum likelihood estimate given only  $\mathbf{y}_t$ , (2) the **dynamics log-likelihood** which is maximized if  $q(\mathbf{x}_t)$  concentrates at around the maximum of  $\mathbb{E}_{q(\mathbf{x}_{t-1})} [\log p(\mathbf{x}_t | \mathbf{x}_{t-1})]$ , and (3) the **entropy term** that expands the posterior and keeps it from collapsing to a point mass.

In order for this recursive estimation to be real-time, we choose the variational posterior over the state  $q(\mathbf{x}_t)$  to be a multivariate normal with diagonal covariance  $\mathcal{N}(\boldsymbol{\mu}_t, \text{diag}(\mathbf{s}_t))$ . Moreover, to amortize the computational cost of optimization to obtain the best  $q(\mathbf{x}_t)$  on each time step, we employ the variational autoencoder architecture (Hinton et al., 1995) to parametrize  $q(\mathbf{x}_t)$  with a recognition model. Intuitively, the recognition model em-

bodies the optimization process of finding  $q(\mathbf{x}_t)$ , that is, it performs an approximate Bayesian filtering computation (in constant time) of (4) according to the objective function  $\mathcal{L}$ . We use a recursive recognition network model that maps  $(q(\mathbf{x}_{t-1}), \mathbf{y}_t)$  to  $q(\mathbf{x}_t)$ . In particular, the recognition model is a deterministic recurrent neural network (RNN; with no extra hidden state):

$$\boldsymbol{\mu}_t, \mathbf{s}_t = \mathbf{h}(\mathbf{y}_t, \mathbf{u}_{t-1}, \boldsymbol{\mu}_{t-1}, \mathbf{s}_{t-1}) \quad (6)$$

We use a simple multi-layer perceptron as  $\mathbf{h}$ . Note that the Markovian architecture of the recognition model reflects the Markovian structure of filtering computation (c.f., smoothing networks often use bidirectional RNN (Sussillo et al., 2016) or graphical models (Archer et al., 2015; Johnson et al., 2016)).

We use the reparameterization trick and stochastic variational Bayes (Rezende et al., 2014; Kingma & Ba, 2014): we rewrite the expectations over  $q$  as expectation over a standard normal random variable, and we use a single sample for each time step. We also impose a Gaussian prior on the state noise (defined by 9d) that is equivalent to a  $\ell_2$  penalty to prevent overestimated state noise. Hence, in practice, we optimize the following objective function (we omit the other variables and parameters for simplicity),

$$\hat{\mathcal{L}} = \log p(\mathbf{y}_t | \tilde{\mathbf{x}}_t) + \mathbb{E}_{q(\mathbf{x}_t)} \log p(\mathbf{x}_t | \tilde{\mathbf{x}}_{t-1}) + H(q(\mathbf{x}_t)) - \frac{1}{2}\gamma\sigma^2 \quad (7)$$

where  $\tilde{\mathbf{x}}_t$  and  $\tilde{\mathbf{x}}_{t-1}$  represents random samples from  $q(\mathbf{x}_t)$  and  $q(\mathbf{x}_{t-1})$  respectively. Note that the remaining expectation over  $q(\mathbf{x}_t)$  has closed form solution for Gaussian state noise. Thus, our method can handle arbitrary observation and dynamics model unlike dual form nonlinear Kalman filtering methods.

Denote the set of all parameters and hyperparameters by  $\Theta$  from the generative, recognition and dynamics parts. The objective in Eq. (7) is differentiable w.r.t.  $\Theta$ . We employ empirical Bayes and optimize the objective function  $\hat{\mathcal{L}}$  through gradient ascent (using Adam (Kingma & Ba, 2014)) implemented within TensorFlow. Algorithm 1 is an overview of the recursive estimation algorithm. We outline the algorithm for a single vector time series, but we can filter multiple sequences with a common state space model simultaneously, in which case the gradients are averaged across the instantiations. Note that this algorithm has constant time complexity per time step.

### 3. Application to Latent Neural Dynamics

Our primary application is real-time neural interfaces where a population of neurons are recorded while a low-dimensional stimulation is delivered (Newman et al., 2015; El Hady, 2016). Latent state space modeling of such neural time series have been successful in describing population

---

**Algorithm 1** Online variational dual estimation (single step)

---

**input**  $\mathbf{y}_t, \mathbf{u}_{t-1}, \boldsymbol{\mu}_{t-1}, \mathbf{s}_{t-1}, \Theta$   
 $\boldsymbol{\mu}_t, \mathbf{s}_t \leftarrow \mathbf{h}(\mathbf{y}_t, \mathbf{u}_{t-1}, \boldsymbol{\mu}_{t-1}, \mathbf{s}_{t-1})$  {recognition}  
 $\tilde{\mathbf{x}}_t \leftarrow \boldsymbol{\mu}_t + \mathbf{s}_t^{1/2} \mathcal{N}(\mathbf{0}, \mathbf{I})$   
 $\tilde{\mathbf{x}}_{t-1} \leftarrow \boldsymbol{\mu}_{t-1} + \mathbf{s}_{t-1}^{1/2} \mathcal{N}(\mathbf{0}, \mathbf{I})$   
 $\hat{\mathcal{L}} \leftarrow \hat{\mathcal{L}}(\Theta; \mathbf{y}_t, \tilde{\mathbf{x}}_t, \tilde{\mathbf{x}}_{t-1}, \mathbf{u}_{t-1})$   
 update  $\Theta$  with  $\nabla_{\Theta} \hat{\mathcal{L}}$  {gradient ascent}  
**output**  $\boldsymbol{\mu}_t, \mathbf{s}_t$  and  $\Theta$

---

dynamics (Macke et al., 2011; Zhao & Park, 2017). Moreover, models of neural computation are often described as dynamical systems (Hopfield, 1982; Dayan & Abbott, 2001; Barak et al., 2013). For example, attractor dynamics where the convergence to one of the attractors represents the result of computation (Wang, 2002). Here we propose a parameterization and tools for visualization of the model suitable for studying neural dynamics and building neural interfaces (Zhao & Park, 2016).

#### 3.1. Parameterization of the generative model

Having in mind high temporal resolution neural spike trains where each time bin has at most one action potential, we describe the case for a point process observation. However, note that our method generalizes to arbitrary observation likelihood appropriate for other modalities, including calcium imaging or local field potentials. Our observed time series  $\mathbf{y}_t$  is a stream of sparse binary vectors. All analysis are done with a 1 ms time bin in this study.

Our generative model assumes that the spike train observation  $\mathbf{y}_t$  is sampled from a probability distribution  $P$  determined by the state  $\mathbf{x}_t$  though a linear-nonlinear map possibly together with extra parameters at each time  $t$ ,

$$\mathbf{y}_t \sim P(f(\mathbf{C}\mathbf{x}_t + \mathbf{b})) \quad (8)$$

where  $f: \mathbb{R} \rightarrow \mathbb{R}^+$  is a point nonlinearity making rates non-negative. We use the canonical link  $f(\cdot) = \exp(\cdot)$  for Poisson likelihood  $P$  in the following study. Note that this model is not identifiable since  $\mathbf{C}\mathbf{x}_t = (\mathbf{C}\mathbf{R})(\mathbf{R}^{-1}\mathbf{x}_t)$  where  $\mathbf{R}$  is an arbitrary invertible matrix. Also, the mean of  $\mathbf{x}_t$  can be traded off with the bias term in  $\mathbf{b}$ . It is straightforward to include more additive exogenous variables, history-filter for refractory period, coupling between processes, and stimulation artifacts (Pillow et al., 2008; Truccolo et al., 2005).

We propose to use a specific parameterization for state dynamics with additive state transition function and locally linear input interaction as a special case of Eq. (2),

$$\mathbf{x}_{t+1} = \mathbf{x}_t + g(\mathbf{x}_t) + \mathbf{B}(\mathbf{x}_t)\mathbf{u}_t + \boldsymbol{\epsilon}_{t+1} \quad (9a)$$

$$g(\mathbf{x}_t) = \mathbf{W}_g \phi(\mathbf{x}_t) \quad (9b)$$

$$\text{vec}(\mathbf{B}(\mathbf{x}_t)) = \mathbf{W}_B \phi(\mathbf{x}_t) \quad (9c)$$

$$\epsilon_t \sim \mathcal{N}(\mathbf{0}, \sigma^2 \mathbf{I}) \quad (9d)$$

$$\mathbf{x}_0 \sim \mathcal{N}(\mathbf{0}, \sigma^2 \mathbf{I}) \quad (9e)$$

where  $\phi(\cdot)$  is a vector of  $r$  continuous basis functions,  $\phi(\cdot) = (\phi_1(\cdot), \dots, \phi_r(\cdot))^\top$ . In this study, we use squared exponential radial basis functions (Roweis & Ghahramani, 2001; Frigola et al., 2014; Sussillo & Barak, 2012; Zhao & Park, 2016),

$$\phi_i(\mathbf{x}) = \exp\left(-\frac{1}{2}\gamma_i\|\mathbf{x} - \mathbf{c}_i\|_2^2\right) \quad (10)$$

with centers  $\mathbf{c}_i$  and corresponding inverse squared kernel width  $\gamma_i$ .

Let  $n, m, p, q, r$  denote the dimensions of observation, latent space, input, the numbers of hidden units and radial basis functions for this specific parameterization. The time complexity of our algorithm is  $\mathcal{O}(mpr + n(m + p + q))$ . If we compare this to an efficient offline algorithm such as PLDS (Macke et al., 2011) run repeatedly for every new observation (“online mode”), its time complexity is  $\mathcal{O}(t \cdot (m^3 + mn))$  per time step at time  $t$  which grows as time passes, making it impractical for real-time application.

### 3.2. Phase portrait analysis

The function  $g(\mathbf{x})$  directly represents the velocity field of an underlying smooth dynamics (1b) in the absence of input (Roweis & Ghahramani, 2001; Zhao & Park, 2016). We visualize the estimated dynamics as phase portrait which consists of the vector field, example trajectories, and estimated dynamical features (namely fixed points) (Strogatz, 2000). We numerically identify candidate fixed points  $\mathbf{x}^*$  that satisfy  $g(\mathbf{x}^*) \approx 0$ . For the simulation studies, we do an affine transformation to orient the phase portrait to match the canonical equations in the main text.

### 3.3. Prediction

The prediction contains both latent trajectory and observation which last for  $T$  steps by sampling from:

$$p(\mathbf{x}_{t+1:T} | \mathbf{y}_{1:t}) = \int p(\mathbf{x}_{t+1:T} | \mathbf{x}_t) q(\mathbf{x}_t) d\mathbf{x}_t \quad (11a)$$

$$p(\mathbf{y}_{t+1:T} | \mathbf{y}_{1:t}) = \int p(\mathbf{y}_{t+1:T} | \mathbf{x}_{t+1:T}) p(\mathbf{x}_{t+1:T} | \mathbf{y}_{1:t}) d\mathbf{x}_{t+1:T} \quad (11b)$$

given estimated parameters without seeing the data  $\mathbf{y}_{t+1:T}$  during these steps.

## 4. Simulated Experiments

For the purposes of visualization, we chose to simulate from two or three dimensional dynamical systems, and generate 200 dimensional Gaussian or spiking observations via state dynamics driven processes. Average firing rate of the

simulated spike trains were kept below 40 Hz.

Many theoretical models have been proposed in neuroscience to represent different schemes of computation. We apply the proposed method to four such low-dimensional models: a ring attractor model as a model of internal head direction representation, an nonlinear oscillator as a model of rhythmic population-wide activity, a biophysically realistic cortical network model for a visual discrimination experiment and a chaotic attractor. We refer to their conventional formulations under different coordinate systems, but our simulations and inferences are all done in Cartesian coordinates.

The approximate posterior distribution is defined recursively in Eq. (6) as diagonal Gaussian with mean and variance determined by corresponding observation, input and previous step via a recurrent neural network. We use one hidden layer MLP in this study. Typically the state noise variance  $\sigma^2$  is unknown and has to be estimated from data. To be consistent with Eq. (9e), we set the starting value of  $\sigma^2$  to be 1, and hence  $\boldsymbol{\mu}_0 = \mathbf{0}, \mathbf{s}_0 = \mathbf{I}$ . We initialize the loading matrix  $\mathbf{C}$  by factor analysis, and column-wisely normalize it by  $\ell_2$  norm every iteration to keep the system identifiable.

### 4.1. Ring attractor

First, we study the following two-variable ring attractor system:

$$\begin{aligned} \tau_r \dot{r} &= r_0 - r \\ \tau_\varphi \dot{\varphi} &= I \end{aligned} \quad (12)$$

where  $\varphi$  represents the direction driven by input  $I$ , and  $r$  is the radial component representing an internal circular variable, such as head direction. We simulate 100 trajectories of 1000 steps with step size 0.1,  $r_0 = 1$ ,  $\tau_r = 1$ ,  $\tau_\varphi = 1$  plus Gaussian noise (std = 0.005). We use strong input (tangent drift) to keep the trajectories flowing around the ring clockwise or counter-clockwise. We use 20 radial basis functions for dynamics model and 100 hidden units for the recognition model.

Figure 1a illustrates one latent trajectory (black) and its variational posterior mean (blue). These two trajectories start at green circle and diamond respectively and end at the red markers. The inference starts near the center (origin) that is relatively far from the true location because the initial posterior mean is set at zero. The final states are very close which implies that the recognition model works well. Figure 1c shows the reconstructed velocity field by the model. We visualize the velocity as colored directional streamlines. We can see the velocity toward the ring attractor and the speed is smaller closer to the ring. The model also identifies a number of fixed points arranged around the ring attractor via numerical roots finding. Figure 1d shows the distribution of posterior means of all data points in the state space.

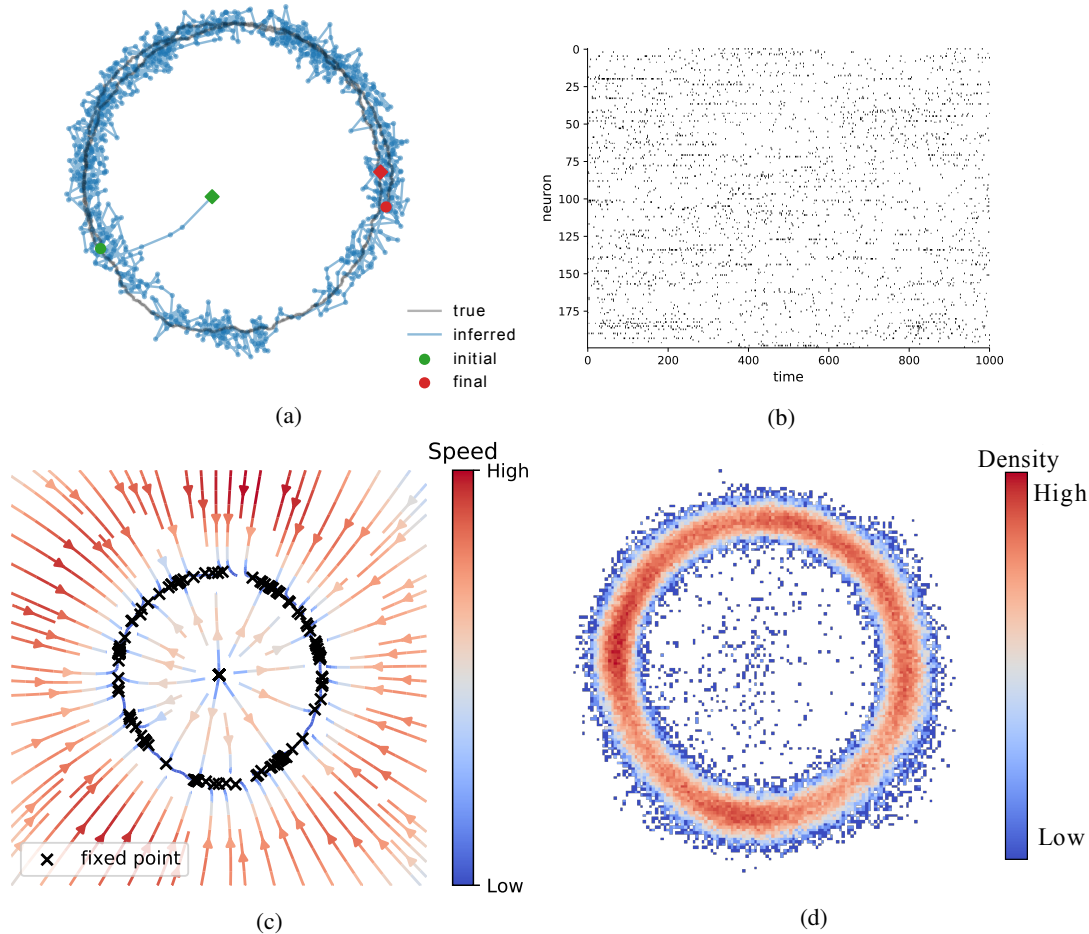


Figure 1: Ring attractor model. (a) One latent trajectory (black) in the training set and the corresponding filtered mean  $\mu_t$  (blue). (b) Raster plot of the observed spike trains corresponding to the left trajectory. (c) Velocity field reconstructed from the trained proposed model. The colored streamlines indicates the speed and the directions. The black crosses are candidate fixed points obtained from inferred dynamics. Note the collection of fixed points around the ring shape. The central fixed point is unstable. (d) Density of the posterior means. The density of inferred means of all trajectories in the training set. The higher it is, the more confidence we have on the inferred dynamics where we have more data.

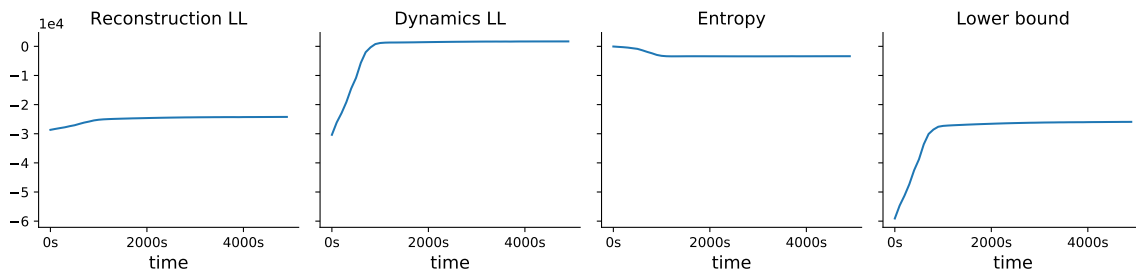


Figure 2: Convergence on the ring attractor. We display the three components of the objective lower bound: reconstruction log-likelihood, dynamics log-likelihood, entropy, and the lower bound itself from Eq. (5).

Figure 2 shows the three components of (5) and the objective lower bound clearly, demonstrating the convergence of the algorithm. We can see each component reaches a plateau within 2000 sec. As the reconstruction and dynamics log-

likelihoods increase, the recognition model and dynamical model are getting more accurate while the decreasing entropy indicates the increasing confidence (inverse posterior variance) on the inferred latent states. The average compu-

tation time of a dual estimation step is 1.6 ms (hardware specification: Intel Xeon E5-2680 2.50GHz, 128GB RAM, no GPU).

## 4.2. Nonlinear oscillator

We use a 2-dimensional relaxation oscillator with the following nonlinear state dynamics:

$$\begin{aligned}\dot{v} &= v(a-v)(v-1) - w + I, \\ \dot{w} &= bv - cw,\end{aligned}\quad (13)$$

where  $v$  is the membrane potential,  $w$  is a recovery variable and  $I$  is the magnitude of stimulus current in modeling single neuron biophysics (Izhikevich, 2007). This model was used to model global brain state that fluctuates between two levels of excitability in anesthetized cortex (Curto et al., 2009). We use the following parameter values  $a = -0.1$ ,  $b = 0.01$ ,  $c = 0.02$  and  $I = 0.1$  to simulate 100 trajectories of 1000 steps with step size 0.5 and Gaussian noise (std=0.002). At this regime, unlike the ring attractor, the spontaneous dynamics is a periodic oscillation, and the trajectory follows a limit cycle.

We use 20 radial basis functions for dynamics model and 100 hidden units for recognition model. While training the model, the input was clamped to zero, and expect the model to learn the spontaneous oscillator.

We also reconstruct the phase portrait (Fig. 3c) comparing to the truth (Fig. 3d). The two dashed lines are the theoretical nullclines of the true model on which the velocity of corresponding dimension is zero. The reconstructed field shows a low speed valley overlapping with the nullcline especially on the right half figure. The intersection of two nullclines is a unstable fixed point. We can see the identified fixed point is close to the intersection.

We run a long-term prediction using the proposed model without seeing the future data  $\mathbf{y}_{t+1:T}$  during these steps ( $T = 1000 = 1$  sec) beginning at the final state of training data. We show the truth and prediction in Figure 4. The upper row is the true latent trajectory and corresponding observations. The lower row is the filtered trajectory and prediction by our proposed method. The light-colored parts are the 500 steps of inference before prediction and the solid-colored parts are 1000 steps truth and prediction. We also show the sample observations from the trained generative model during the prediction period.

One of the popular latent process modeling tools for point process observation that can make prediction is Poisson Linear Dynamical System (PLDS) (Macke et al., 2011) which assumes latent linear dynamics. We compare PLDS fit with EM on its long-term prediction on both the states and spike trains (Fig. 4).

## 4.3. Fixed point attractor for decision-making

Perceptual decision-making paradigm is a well-established cognitive task where typically a low-dimensional decision variable needs to be integrated over time, and subjects are close to optimal in their performance. To understand how the brain implements such neural computation, many competing theories have been proposed (Barak et al., 2013; Mante et al., 2013; Ganguli et al., 2008; Wang, 2002; Wong & Wang, 2006). We test our method on a simulated biophysically realistic cortical network model for a visual discrimination experiment (Wang, 2002). In the model, there are two excitatory subpopulations that are wired with slow recurrent excitation and feedback inhibition to produce attractor dynamics with two stable fixed points. Each fixed point represents the final perceptual decision, and the network dynamics amplify the difference between conflicting inputs and eventually generates a binary choice.

We subsampled 480 neurons out of 1600 excitatory neurons from the simulation to be observed by our algorithm. The simulated data is organized into decision-making trials where each trial lasts for 2 sec and with different strength of visual evidence, controlled by ‘‘coherence’’. Our method with 20 basis functions learned the dynamics from 140 training trials (20 per coherence  $c = -1, -0.2, -0.1, 0, 0.1, 0.2, 1$  where max is 100). We visualize the velocity field at zero stimulus as colored streamlines in Figure 5. The left panel is the estimated velocity field and the right panel is the theoretical velocity field of a theoretically reduced model (Wong & Wang, 2006). Note that the spiking neuron model where the simulation comes from is different from the reduced model. Here we want to show that our method can provide a qualitatively similar result to the theoretical work which reduces the dimensionality and complexity of the original network.

## 4.4. Chaotic dynamics

Chaotic dynamics (or edge-of-chaos) has been postulated to support asynchronous states in the cortex, and neural computation over time by generating rich temporal patterns (Maass et al., 2002; Laje & Buonomano, 2013). We consider the 3-dimensional standard Lorenz attractor as an example chaotic system. We simulate 216 latent trajectories from:

$$\dot{x} = 10(y-x), \quad \dot{y} = x(28-z)-y, \quad \dot{z} = xy - \frac{8}{3}z. \quad (14)$$

The initial states of the trajectories are evenly-spaced. We discard the first 500 transient steps of each trajectory and then use the following 1000 steps. We generate 200-dimensional Gaussian observations driven by the trajectories. Figure 6 shows the inference and prediction. We continue simulating a trajectory for 2000 more steps from the final state where the training data end, and predict the latent state through the proposed model. The black lines

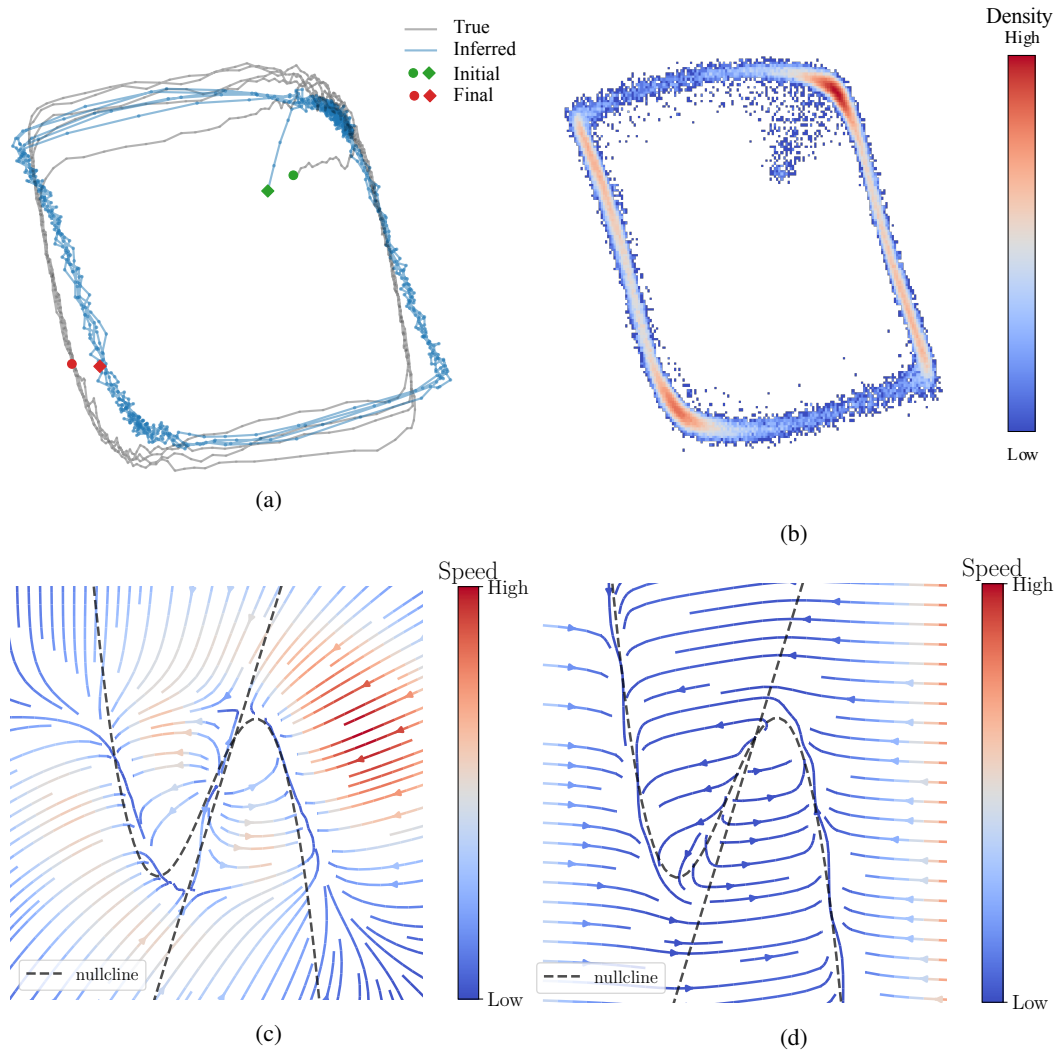


Figure 3: Nonlinear oscillator (FitzHugh-Nagumo) model. (a) One latent trajectory in the training set and its variational posterior mean (1000 steps). (b) Density of posterior means. Most of the inferred trajectory lie on the oscillation path. (c) Velocity field reconstructed by the inferred dynamical system. (d) Velocity field of the true dynamical system. The dashed lines are two nullclines of the true model on which the gradients are zero so as the velocity.

show the three dimensions of true state respectively and the red lines are the model-prediction. We reset the prediction back to the true state every 500 steps.

We also tried to apply the same data to the unscented Kalman filter (UKF; result not shown) for the dual estimation. However, the UKF is not flexible with arbitrary likelihood e.g. Poisson. Even when we used true dynamics equation instead of the radial basis function network, it suffers numerical singularity issues, requires fine hyperparameter tuning, and initialization close to the true value.

## 5. Discussion

New and future technologies for recording the activity of large neural populations during meaningful behavior will provide exciting opportunities for investigating the neural computations that underlie perception, cognition, and decision-making. However, the datasets provided by these technologies currently require sophisticated offline analyses that slow down the scientific cycle of experiment, data analysis, hypothesis generation, and further experiment. Moreover, in closed-loop neurophysiological setting, real-time adaptive algorithms are extremely valuable. We proposed an online algorithm for recursive variational Bayesian inference for both system identification and filtering that can

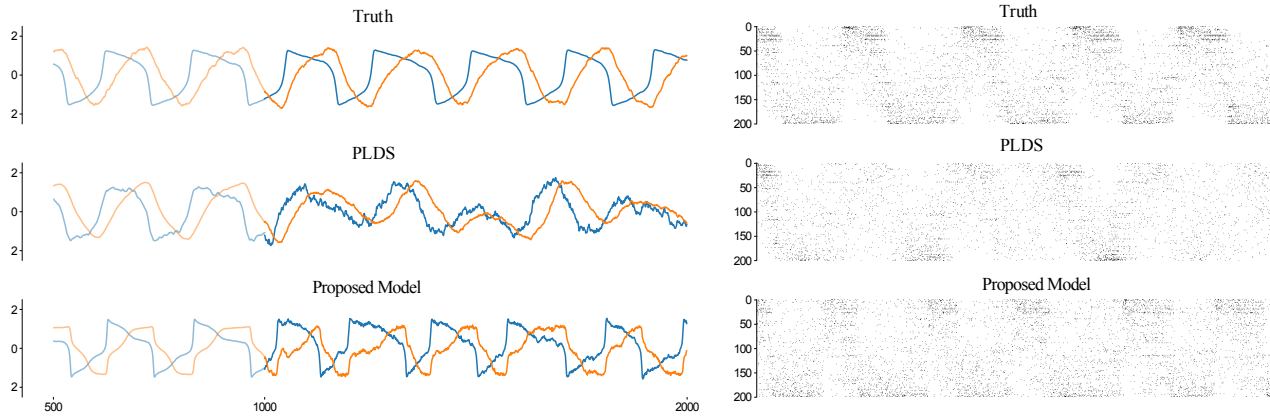


Figure 4: Long term (1000-step) prediction of the trajectory and sampled spike trains compared to ground truth from Figure 3a. Note that PLDS fails to predict long term due to its linear dynamics assumption. A linear dynamical system without noise can only produce damped oscillations.

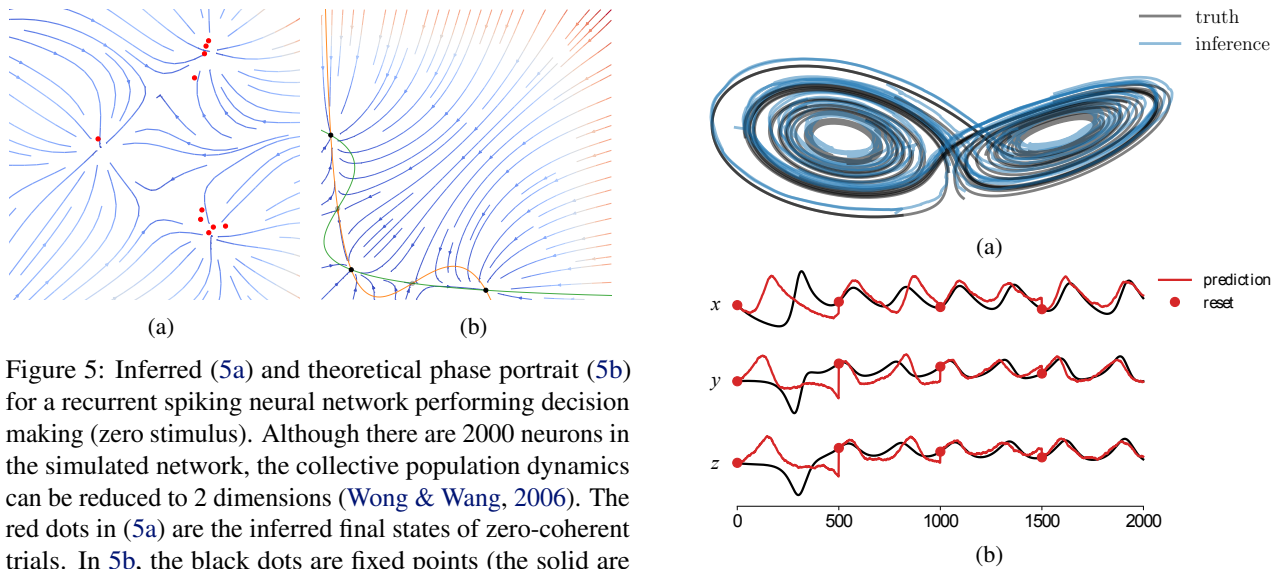


Figure 5: Inferred (5a) and theoretical phase portrait (5b) for a recurrent spiking neural network performing decision making (zero stimulus). Although there are 2000 neurons in the simulated network, the collective population dynamics can be reduced to 2 dimensions (Wong & Wang, 2006). The red dots in (5a) are the inferred final states of zero-coherent trials. In 5b, the black dots are fixed points (the solid are stable and the gray are unstable) Although the absolute arrangement is dissimilar, the relative topology and relation of the three identified fixed points show correspondence.

greatly impact neuroscience research and biomedical engineering. Our algorithm is flexible—allows wide range of likelihood and dynamics, computationally tractable, and produces interpretable visualizations of complex collective network dynamics.

This work opens many avenues for future work. One direction is to apply this model to large-scale neural recording from a behaving animal. We hope that further development would enable on-the-fly analysis of high-dimensional neural spike train during electrophysiological experiments. Clinically, a nonlinear state space model provides a basis for feedback control as a potential treatment for neurological

Figure 6: Lorenz attractor. (6a) The true latent trajectories and their inferences. (6b) We simulate the system for 2000 more steps continuing at the final state where the training data end and predict the latent state through the trained model. The black lines show the three dimensions of true state respectively and the red lines are the model-prediction. We reset the prediction back to the true state every 500 steps.

diseases that arise from diseased dynamical states. Another direction to improve is the slow convergence. In full on-line mode, the current training takes a significant time to have a descent predictive performance. We can use quick offline training to initialize before switching to online mode to expedite the convergence.

## References

- Archer, Evan, Park, Il Memming, Buesing, Lars, Cunningham, John, and Paninski, Liam. Black box variational inference for state space models. *ArXiv e-prints*, November 2015.
- Barak, Omri, Sussillo, David, Romo, Ranulfo, Tsodyks, Misha, and Abbott, L. F. From fixed points to chaos: three models of delayed discrimination. *Progress in neurobiology*, 103:214–222, April 2013. ISSN 1873-5118. doi: 10.1016/j.pneurobio.2013.02.002.
- Broderick, Tamara, Boyd, Nicholas, Wibisono, Andre, Wilson, Ashia C., and Jordan, Michael I. Streaming variational bayes. In Burges, C. J. C., Bottou, L., Welling, M., Ghahramani, Z., and Weinberger, K. Q. (eds.), *Advances in Neural Information Processing Systems 26*, pp. 1727–1735. Curran Associates, Inc., 2013.
- Curto, Carina, Sakata, Shuzo, Marguet, Stephan, Itskov, Vladimir, and Harris, Kenneth D. A simple model of cortical dynamics explains variability and state dependence of sensory responses in Urethane-Anesthetized auditory cortex. *The Journal of Neuroscience*, 29(34):10600–10612, August 2009. ISSN 1529-2401. doi: 10.1523/jneurosci.2053-09.2009.
- Dayan, Peter and Abbott, L. F. *Theoretical neuroscience: computational and mathematical modeling of neural systems*. Massachusetts Institute of Technology Press, 2001. ISBN 9780262041997.
- El Hady, Ahmed. *Closed Loop Neuroscience*. Academic Press, 2016. ISBN 9780128024522.
- Frigola, Roger, Chen, Yutian, and Rasmussen, Carl. Variational gaussian process State-Space models. In Ghahramani, Z., Welling, M., Cortes, C., Lawrence, N. D., and Weinberger, K. Q. (eds.), *Advances in Neural Information Processing Systems 27*, pp. 3680–3688. Curran Associates, Inc., 2014.
- Ganguli, Surya, Bisley, James W., Roitman, Jamie D., Shadlen, Michael N., Goldberg, Michael E., and Miller, Kenneth D. One-dimensional dynamics of attention and decision making in LIP. *Neuron*, 58(1):15–25, April 2008. ISSN 1097-4199. doi: 10.1016/j.neuron.2008.01.038.
- Ghahramani, Zoubin and Roweis, Sam T. Learning nonlinear dynamical systems using an EM algorithm. In Kearns, M. J., Solla, S. A., and Cohn, D. A. (eds.), *Advances in Neural Information Processing Systems 11*, pp. 431–437. MIT Press, 1999.
- Golub, Matthew D., Chase, Steven M., and Yu, Byron M. Learning an internal dynamics model from control demonstration. *JMLR workshop and conference proceedings*, pp. 606–614, 2013. ISSN 1938-7288.
- Haykin, S. and Principe, J. Making sense of a complex world [chaotic events modeling]. *IEEE Signal Processing Magazine*, 15(3):66–81, May 1998. ISSN 10535888. doi: 10.1109/79.671132.
- Haykin, Simon S. *Kalman filtering and neural networks*. Wiley, 2001. ISBN 0471221546.
- Hinton, G. E., Dayan, P., Frey, B. J., and Neal, R. M. The “wake-sleep” algorithm for unsupervised neural networks. *Science*, 268(5214):1158–1161, May 1995. ISSN 0036-8075. doi: 10.1126/science.7761831.
- Ho, Y. and Lee, R. A Bayesian approach to problems in stochastic estimation and control. *IEEE Transactions on Automatic Control*, 9(4):333–339, October 1964. ISSN 0018-9286. doi: 10.1109/tac.1964.1105763.
- Hopfield, J. J. Neural networks and physical systems with emergent collective computational abilities. *Proceedings of the National Academy of Sciences*, 79(8):2554–2558, April 1982. ISSN 1091-6490.
- Izhikevich, Eugene M. *Dynamical systems in neuroscience: the geometry of excitability and bursting*. Computational neuroscience. MIT Press, 2007.
- Johnson, Matthew, Duvenaud, David K, Wiltchko, Alex, Adams, Ryan P, and Datta, Sandeep R. Composing graphical models with neural networks for structured representations and fast inference. In Lee, D. D., Sugiyama, M., Luxburg, U. V., Guyon, I., and Garnett, R. (eds.), *Advances in Neural Information Processing Systems 29*, pp. 2946–2954. Curran Associates, Inc., 2016.
- Karl, Maximilian, Soelch, Maximilian, Bayer, Justin, and van der Smagt, Patrick. Deep variational Bayes filters: Unsupervised learning of state space models from raw data. In *5th International Conference on Learning Representations*, 2017.
- Kingma, Diederik P. and Ba, Jimmy. Adam: A method for stochastic optimization. *CoRR*, abs/1412.6980, 2014.
- Ko, Jonathan and Fox, Dieter. GP-BayesFilters: Bayesian filtering using gaussian process prediction and observation models. *Autonomous Robots*, 27(1):75–90, July 2009. doi: 10.1007/s10514-009-9119-x.
- Krishnan, Rahul G., Shalit, Uri, and Sontag, David. Deep Kalman filters. *arXiv*, abs/1511.05121, November 2015.
- Krishnan, Rahul G., Shalit, Uri, and Sontag, David. Structured inference networks for nonlinear state space models. In *Thirty-First AAAI Conference on Artificial Intelligence*, February 2017.

- Laje, Rodrigo and Buonomano, Dean V. Robust timing and motor patterns by taming chaos in recurrent neural networks. *Nat Neurosci*, 16(7):925–933, July 2013. ISSN 1097-6256. doi: 10.1038/nn.3405.
- Maass, Wolfgang, Natschläger, Thomas, and Markram, Henry. Real-time computing without stable states: A new framework for neural computation based on perturbations. *Neural Computation*, 14:2531–2560, 2002.
- Macke, Jakob H., Buesing, Lars, Cunningham, John P., Yu, Byron M., Shenoy, Krishna V., and Sahani, Maneesh. Empirical models of spiking in neural populations. In Shawe-Taylor, J., Zemel, R. S., Bartlett, P. L., Pereira, F., and Weinberger, K. Q. (eds.), *Advances in Neural Information Processing Systems 24*, pp. 1350–1358. Curran Associates, Inc., 2011.
- Mante, Valerio, Sussillo, David, Shenoy, Krishna V., and Newsome, William T. Context-dependent computation by recurrent dynamics in prefrontal cortex. *Nature*, 503(7474):78–84, November 2013. ISSN 0028-0836. doi: 10.1038/nature12742.
- Mattos, Cesar Lincoln C., Dai, Zhenwen, Damianou, Andreas, Forth, Jeremy, Barreto, Guilherme A., and Lawrence, Neil D. Recurrent gaussian processes. *International Conference on Learning Representations (ICLR)*, 2016.
- Newman, Jonathan P., Fong, Ming-fai, Millard, Daniel C., Whitmire, Clarissa J., Stanley, Garrett B., and Potter, Steve M. Optogenetic feedback control of neural activity. *eLife*, 2015. ISSN 2050-084X. doi: 10.7554/elife.07192.001.
- Pillow, J. W., Shlens, J., Paninski, L., Sher, A., Litke, A. M., and Chichilnisky, E. J. Simoncelli, E. P. Spatio-temporal correlations and visual signaling in a complete neuronal population. *Nature*, 454:995–999, 2008.
- Rezende, Danilo J., Mohamed, Shakir, and Wierstra, Daan. Stochastic backpropagation and approximate inference in deep generative models. In *International Conference on Machine Learning*, May 2014.
- Roweis, Sam and Ghahramani, Zoubin. *Learning nonlinear dynamical systems using the expectation-maximization algorithm*, pp. 175–220. John Wiley & Sons, Inc, 2001. ISBN 0-471-22154-6.
- Särkkä, Simo. *Bayesian filtering and smoothing*. Cambridge University Press, 2013. ISBN 9781107619289.
- Strogatz, Steven H. *Nonlinear dynamics and chaos : with applications to physics, biology, chemistry, and engineering*. Paperback, January 2000.
- Sussillo, David and Barak, Omri. Opening the black box: Low-Dimensional dynamics in High-Dimensional recurrent neural networks. *Neural Computation*, 25(3):626–649, December 2012. doi: 10.1162/neco\_a.00409.
- Sussillo, David, Jozefowicz, Rafal, Abbott, Larry F., and Pandarinath, Chethan. LFADS - latent factor analysis via dynamical systems. *arXiv*, abs/1608.06315, August 2016.
- Truccolo, Wilson, Eden, Uri T., Fellows, Matthew R., Donoghue, John P., and Brown, Emery N. A point process framework for relating neural spiking activity to spiking history, neural ensemble, and extrinsic covariate effects. *Journal of Neurophysiology*, 93(2):1074–1089, February 2005. ISSN 0022-3077. doi: 10.1152/jn.00697.2004.
- Valpola, Harri and Karhunen, Juha. An unsupervised ensemble learning method for nonlinear dynamic State-Space models. *Neural Computation*, 14(11):2647–2692, November 2002. doi: 10.1162/089976602760408017.
- Wan, E. A. and Van Der Merwe, R. The unscented Kalman filter for nonlinear estimation. In *Proceedings of the IEEE 2000 Adaptive Systems for Signal Processing, Communications, and Control Symposium (Cat. No.00EX373)*, pp. 153–158. IEEE, August 2000. ISBN 0-7803-5800-7. doi: 10.1109/asspcc.2000.882463.
- Wan, Eric A. and Nelson, Alex T. *Dual extended Kalman filter methods*, pp. 123–173. John Wiley & Sons, Inc, 2001. ISBN 0-471-22154-6.
- Wang, Xiao-Jing. Probabilistic decision making by slow reverberation in cortical circuits. *Neuron*, 36(5):955–968, dec 2002. ISSN 08966273. doi: 10.1016/S0896-6273(02)01092-9.
- Watter, Manuel, Springenberg, Jost, Boedecker, Joschka, and Riedmiller, Martin. Embed to control: A locally linear latent dynamics model for control from raw images. In Cortes, C., Lawrence, N. D., Lee, D. D., Sugiyama, M., and Garnett, R. (eds.), *Advances in Neural Information Processing Systems 28*, pp. 2746–2754. Curran Associates, Inc., 2015.
- Wong, Kong-Fatt and Wang, Xiao-Jing. A recurrent network mechanism of time integration in perceptual decisions. *The Journal of Neuroscience*, 26(4):1314–1328, January 2006. ISSN 1529-2401. doi: 10.1523/jneurosci.3733-05.2006.
- Zhao, Yuan and Park, Il Memming. Interpretable nonlinear dynamic modeling of neural trajectories. In *Advances in Neural Information Processing Systems (NIPS)*, 2016.

Zhao, Yuan and Park, Il Memming. Variational latent Gaussian process for recovering single-trial dynamics from population spike trains. *Neural Computation*, 29(5), May 2017. doi: 10.1162/NECO.a.00953.